Surface wave processes in air-sea interaction

Stephen E. Belcher[1], Alan L. M. Grant[1], Kirsty E. Hanley[1] and Peter P. Sullivan[2]

[1] *Department of Meteorology,*
University of Reading, United Kingdom
[2] *National Center for Atmospheric Research, Boulder, Colorado*
Corresponding author: s.e.belcher@reading.ac.uk

ABSTRACT

We review briefly recent progress on understanding the role of surface waves on the marine atmospheric boundary layer and the ocean mixed layer and give a global perspective on these processes by analysing ERA-40 data. Ocean surface waves interact with the marine atmospheric boundary layer in two broad regimes: (i) the conventional wind-driven wave regime, when fast winds blow over slower moving waves, yielding wave growth, and (ii) a wave-driven wind regime when long wavelength swell propagates under low winds, and generate a wave-driven jet in the lower part of the marine boundary layer. Analysis of ERA-40 data indicates that the wave-driven wind regime is as prevalent as the conventional wind-driven wave regime. Ocean surface waves also change profoundly mixing in the ocean mixed layer through generation of Langmuir circulation. Results from large-eddy simulation are used here to develop a scaling for the resulting Langmuir turbulence, which is a necessary step in developing a parameterisation of the process. ERA-40 data is then used to show that the Langmuir regime is the predominant regime over much of the global ocean, providing a compelling motivation for parameterising this process in ocean general circulation models.

1 Introduction

Ocean surface waves have profound dynamical effects on the marine atmospheric boundary layer and the ocean mixed layer that are only just beginning to be fully appreciated. Here two mechanisms are reviewed briefly: the effects of fast moving swell on the atmospheric boundary layer; and the effects of waves in generating mixing through Langmuir turbulence in the ocean mixed layer. (We note that waves also have a substantial effect on the mean current profile in the mixed layer: e.g. Polton et al., 2005). Estimates are made of the global extent of these processes by analysing the ERA-40 data on ocean waves and air-sea coupling.

Fig. 1 shows global climatologies of the surface wind and waves derived from the ERA-40 data. The ERA-40 is constructed from re-analysis using the ECMWF forecasting system with data assimilation (Uppala et al., 2005). Surface waves are computed in the model using the WAM model with assimilated observations from buoys and satellites (Lionello et al., 1992). The surface wind fields show strong zonal winds in the mid-latitude storm tracks and the subtropical trade winds. This leads to mean significant wave heights of 3 m or more in the storm tracks. The peak wave speed is defined to be the wave speed at the peak in the wave spectrum and is seen to have a strong zonal variation with smaller values on the western edges of the ocean basins increasing towards the east, because the fetch of the waves is limited on the western edges of the ocean basins limiting the growth of fast-moving long-wavelength waves. Particularly fast-moving long wavelength waves propagate out of their region of generation in the Southern Ocean storm tracks towards the subtropics in the eastern Indian and Pacific Oceans as swell. As we shall see these patterns inform the interactions of surface waves with the atmospheric and oceanic boundary layers.

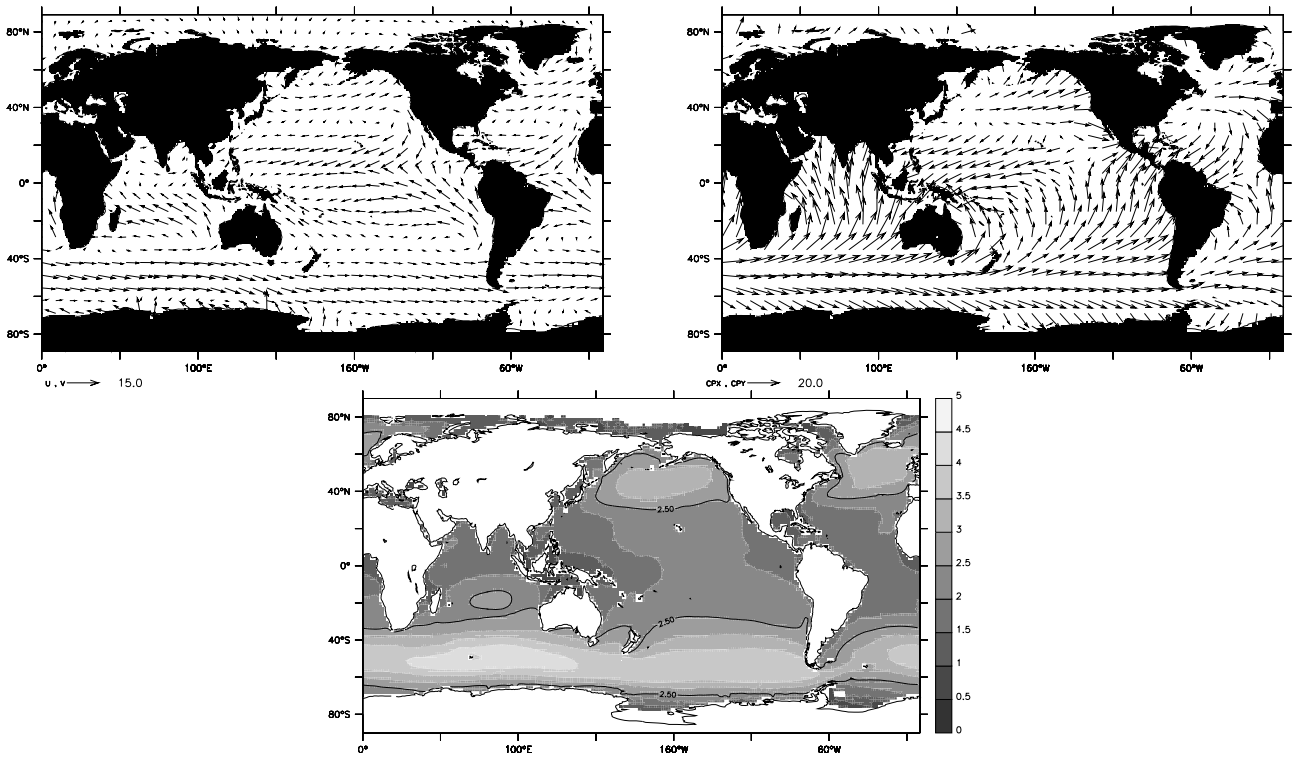

Figure 1: Global climatologies derived from the ERA-40 data averaged over 1958 – 2001 of 10 *m wind speed and direction in m* s^{-1} *(top left), peak phase speed and direction in m* s^{-1} *(top right) and significant wave height in m (bottom).*

2 Wave-driven winds in the marine atmospheric boundary layer

There are two distinct regimes of dynamical interaction between surface waves and the atmospheric boundary layer. When the waves have shorter wavelengths, they propagate more slowly than the surface wind speed. The waves then extract momentum and energy from the wind, leading to wave growth. This is the *wind-driven wave regime*. This regime has been extensively studied and theory and observations are now well developed. This regime is often represented through a Charnock relation to parameterise the drag of the waves on the boundary layer winds.

When long-wavelength swell propagates into regions of low surface winds, the waves then give up energy and momentum to the wind, thereby generating a low-level wind jet in the atmospheric boundary layer. This is the *wave-driven wind regime*. Although this regime has been recognised for some time (see Harris, 1966, for early wave tank measurements), it is much less well understood. In recent years evidence of the upwards momentum flux has been accumulating from observational studies (e.g. Grachev and Fairall, 2001; Smedman et al., 1999; Edson et al., 2007) and from theory (e.g. Cohen and Belcher, 1999; Kudryavtsev and Makin, 2004). Sullivan et al. (2008) have invigorated the study of this regime by demonstrating its importance during the CBLAST observational campaign (Edson et al., 2007).

Hanley and Belcher (2008) describe how the usual Ekman dynamics are totally changed by the upwards momentum flux from the waves. It leads to momentum convergence and the production of a low-level wind jet, which turbulent fluxes tend to try to diffuse away. The Coriolis force associated with the jet balances the friction and pressure gradient forces when the super-geostrophic wind jet turns towards the high pressure – the opposite direction to the normal Ekman spiral! Hanley and Belcher (2008) also show that the sign of the total momentum flux from the sea surface, which is the sum in these circumstances of an upwards wave-induced momentum flux and a downwards turbulent momentum flux, can be determined from the inverse wave age,

$(U\cos\theta)/c_p$, where $U\cos\theta$ is the mean 10 m wind component perpendicular to the waves, and c_p is the phase speed of the waves at the peak in the wave spectrum. The sign reversal occurs when $(U\cos\theta)/c_p$ drops below about 0.15 – 0.2, in rough agreement with the ocean measurements of Grachev and Fairall (2001).

Fig. 2 therefore shows a climatology computed from ERA-40 of the inverse wave age. The inverse wave age is

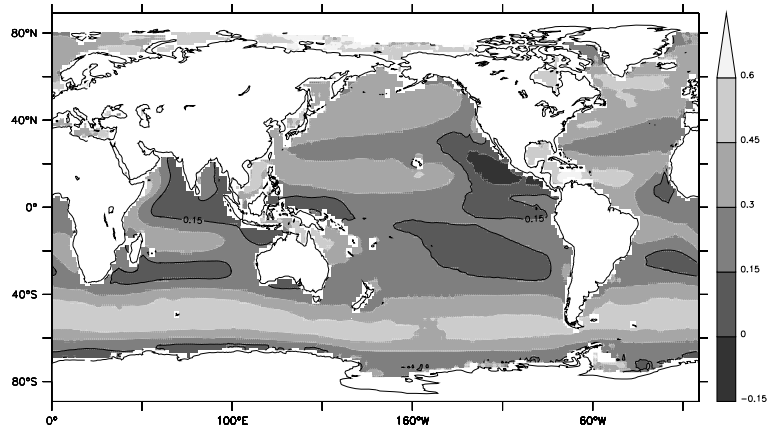

Figure 2: Climatology of inverse wave age computed from the ERA-40 data averaged over 1958 – 2001.

generally high in the storm tracks, indicating wave-driven winds. It is notable that nowhere in the climatology is the inverse wave age even close to the value of 0.83 associated with a fully developed sea. The reason is that the sea state in the storm tracks is mixed wind sea and swell because of the succession of cyclonic storms that generate the waves. A striking feature of Fig. 2 is the existence of large regions of the oceans where $(U\cos\theta)/c_p < 0.15$, particularly the eastern edges of the tropical ocean basins, indicating swell propagating under low winds, so that upward momentum transfer, and wave-driven winds, is expected to be predominant. The wave-driven wind regime appears to be as prevalent in the world's oceans as the wind-driven wave regime.

3 Characteristics of Langmuir turbulence in the ocean mixed layer

Langmuir circulations are generally thought to result from the interaction between the Stokes drift, associated with surface waves, and fluctuations in vorticity within the mixed layer (Craik and Leibovich, 1976). The effect of the Stokes drift has been parametrized in large-eddy simulations using the Craik and Leibovich (1976) vortex force, e.g. Skyllingstad and Denbo (1995), McWilliams et al. (1997). A feature of these simulations is that the variance of the vertical component of the fluctuating current, σ_w^2, normalised by the surface friction velocity, u_*, is much larger than observed in normal shear driven turbulence. This is in agreement with limited observations of σ_w^2 published by D'Asaro (2001) and Tseng and D'Asaro (2004). This leads to faster deepening of the mixed layer. Here we report analyses of new large-eddy simulations that aims to provide a scaling for the Langmuir turbulence, as a first step to parameterization in simpler models. Further details can be found in Grant and Belcher (2009).

The first step in deriving the scaling is to consider the turbulence kinetic energy budget (TKE), including the effects of Stokes drift, can be written as,

$$-\overline{u'w'}\frac{\partial\overline{U}}{\partial z}-\overline{v'w'}\frac{\partial\overline{V}}{\partial z}-\overline{u'w'}\frac{du_s}{dz}+\overline{w'b'}-\frac{\partial}{\partial z}\left(\overline{w'E}+\frac{1}{\rho}\overline{w'p'}\right)-\varepsilon=0 \qquad (1)$$

where $\rho\overline{u'w'}$ and $\rho\overline{v'w'}$ are the components of the surface stress, ρ is the density of sea water, $\overline{U}$ and $\overline{V}$ are the components of the mean current, u_s is the Stokes drift, b is the buoyancy, E is the TKE, p is the pressure and ε is the dissipation rate. Overbars represent an average and $'$ a fluctuation from the average.

The terms on the right-hand side of Eq. 1 are production due to current shear (first and second terms), production due to Stokes shear (third term), buoyancy production/destruction (fourth term), turbulent and pressure transport (fifth term) and the dissipation of TKE by molecular viscosity (final term).

Fig. 3 shows an example of the TKE budget from one of our large-eddy simulations (LES) that includes the effects of Stokes drift. The main production of TKE is through the Stokes shear term, with production of TKE by the current shear being small. The production due to Stokes shear is confined to the upper part of the mixed layer, where the Stokes shear is significant. The transport term removes TKE from the layer of Stokes-shear production to the rest of the mixed layer which Polton and Belcher (2007) show to be associated with strong downwelling jets. This redistribution of TKE means that the dissipation rate is significant throughout the depth of the mixed layer, not just in the layer of Stokes shear. In this simulation the buoyancy term is negative (i.e. consumes TKE) throughout the mixed layer, and is associated with entrainment.

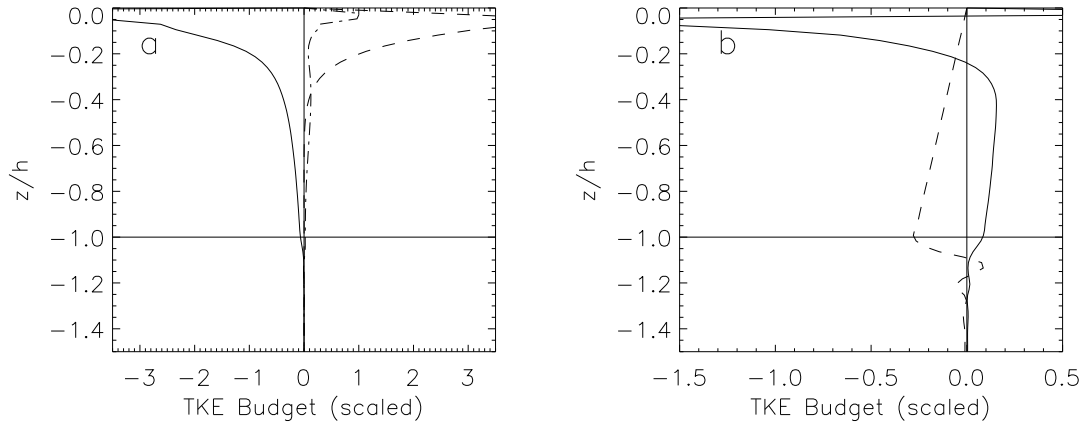

Figure 3: Example of TKE budget of Langmuir turbulence from LES (a) Solid curve, dissipation, dashed curve, Stokes-shear production, dot-dashed curve, current-shear production. (b) Solid curve, transport, dashed curve, buoyancy.

The dominant terms in the TKE budget are therefore the Stokes shear production of TKE, turbulent transport of TKE so produced and the dissipation of TKE. A scaling can be obtained for the Langmuir turbulence as follows. In high Reynolds number turbulence the magnitude of the dissipation rate is $\sim w_{*L}^3/\ell$, where w_{*L} is the velocity scale for the large eddies that are responsible for transports in the mixed layer, and ℓ is the length scale of these large eddies (Tennekes and Lumley, 1972). Here the turbulence length scale is estimated to be $\ell \sim h$ because strong transport of TKE ensures dissipation occurs throughout the depth of the mixed layer. The Stokes-shear production, averaged over the depth of the mixed layer is $\sim \left(u_*^2 u_{s0}/\delta\right) \times \delta/h$, where u_{s0} is the surface Stokes drift and δ decay scale for the effects of surface waves. The mixed layer average of the Stoke production is considered here because of the redistribution of TKE by the transport term. Equating the magnitudes of the Stokes-shear production and dissipation gives,

$$w_{*L} = \left(u_*^2 u_{s0}\right)^{1/3} = \frac{1}{La_t^{2/3}} u_* \tag{2}$$

where $La_t = \left(u_*/u_{s0}\right)^{1/2}$ is the turbulent Langmuir number.

We judge the success of this scaling by investigating profiles of dissipation normalised on w_{*L}^3/h for various values of the Langmuir number. Fig. 4 shows profiles of the dissipation rate scaled by w_{*L}^3/h for different values of La_t. For $La_t = \left(u_*/u_{s0}\right)^{\frac{1}{2}} < 0.5$ the dissipation rate profiles normalised on w_{*L}^3/h collapse onto a single curve independent of La_t. We conclude that (i) when $La_t < 0.5$ it is possible to speak of Langmuir turbulence as a

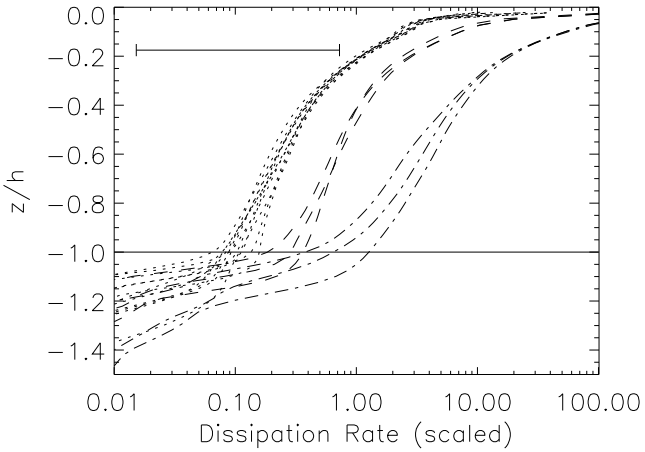

Figure 4: Profiles of dissipation rate, scaled by w_{*L}^3/h, as a function of non-dimensional depth, z/h. Dot-dash curves have $La_t = 1.5$, the dashed curves, $La_t = 0.8$ and dotted curves $La_t < 0.5$. The horizontal line at $z/h = -0.2$ shows the variation in the scale w_{*L}^3/h for the simulations with $La_t < 0.5$.

distinct turbulent flow regime with its own scaling distinct from that of shear-driven turbulence and (ii) w_{*L} and h are the appropriate scaling variables for Langmuir turbulence.

Fig. 5 shows $\varepsilon h/u_*^3$ in the middle of the mixed layer as a function of La_t. For $La_t < 0.5$ the results vary as

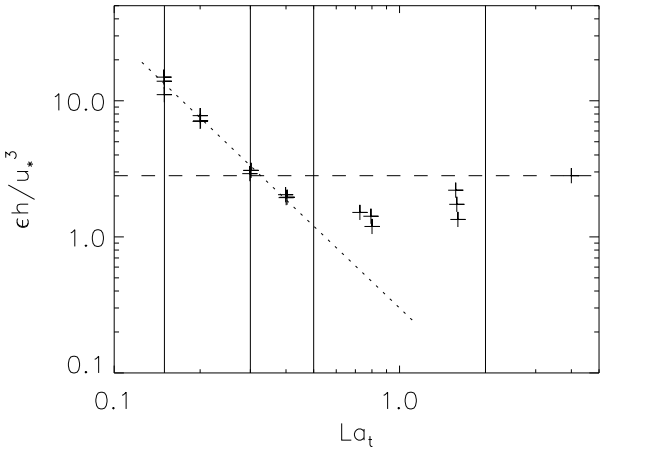

Figure 5: The dissipation rate at $z/h = -0.5$, non-dimensionalised by u_*^3/h as a function of La_t. The dotted line shows $\varepsilon h/u_*^3 \propto 1/La_t^2$ which is consistent with ε scaling with w_{*L}^3/h. The horizontal dashed line shows the non-dimensional dissipation for a shear-driven mixed layer without wave effects. The vertical lines show the ranges of La_t considered in Fig. 6.

$1/La_t^2$, which is consistent with Eq. 2. Between $La_t = 0.5$ and 2 the dissipation rate reaches a minimum and increases towards the value appropriate to the normal shear driven mixed layer for $La_t > 2$. For reference $La_t \approx 0.3$ corresponds to a fully developed wind-driven sea.

ERA-40 data have been used to calculate the turbulent Langmuir number globally to make an assessment as

to the importance of Langmuir turbulence in the oceanic mixed layer, and whether parametrizations should be developed to represent its effects in large-scale ocean models. Fig. 6 shows maps of the frequency of occurrence of the ranges of La_t marked in Fig. 5. These maps show that $La_t < 2$ occurs over a large proportion of the ocean,

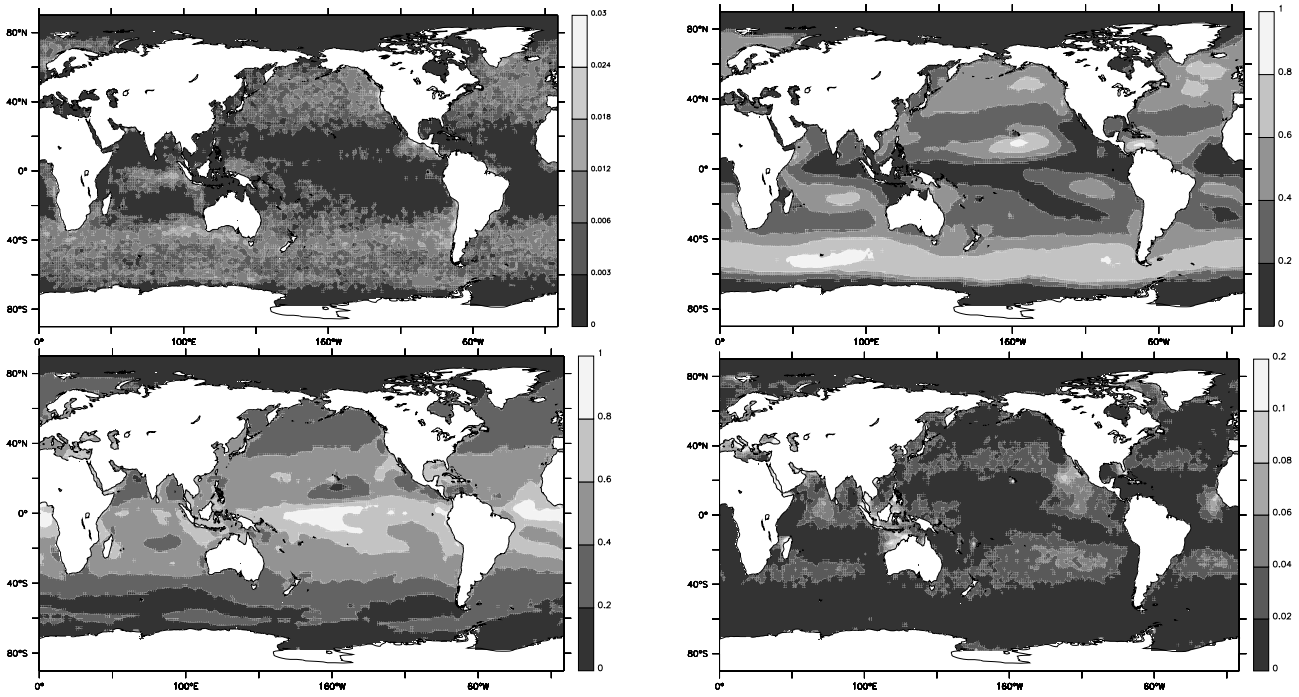

Figure 6: Maps of the frequency of occurrence of ranges of La_t for the year 2001. (Upper left) $0.15 < La_t < 0.3$*, the grey scale runs from 0 to 0.03, (upper right)* $0.3 < La_t < 0.5$*, the grey scale runs from 0 to 1, (lower left)* $0.5 < La_t < 2$*, the grey scale runs from 0 to 1, (lower right),* $La_t > 2$*, the grey scale runs from 0 to 0.2.*

suggesting that the effects of waves on mixing in the oceanic mixed layer are important and should be accounted for in parametrizations. The lower right panel in Fig. 6 suggests that wind and wave conditions are such that the occurrence of classic shear driven turbulence is likely to be rare. Although Fig. 6 shows that wave effects are likely to be important it does not show the occurrence of convective mixed layers, driven by surface heat fluxes, in which convectively generated turbulence may be the dominant mechanism for mixing.

4 Summary

In conditions of low-wind and fast-swell the total air-sea momentum flux reverses sign from positive (into the waves) to negative (out of the waves). Hanley and Belcher (2008) show that this sign reversal occurs when the inverse wave age, $(U\cos\theta)/c_p$, drops below about 0.15 – 0.2. This condition provides a first practical estimate of wave-driven winds and has been used to determine the global prevalence of this regime. The results presented here demonstrate the importance of the wave-driven wind regime across the world's oceans indicating that upward momentum transfer should be included in large-scale models.

The scaling described here is a first step in developing parametrizations of mixing by Langmuir turbulence that can be used in large-scale ocean models. In the popular K Profile Parametrization (KPP) scheme of Large et al. (1994) similarity scalings are used to determine eddy diffusivities and other terms in the flux-gradient relationship. In order to incorporate the effects of Stokes drift into such a scheme an understanding of the scaling of Langmuir turbulence is required. ERA-40 data demonstrate the global importance of the Langmuir turbulence regime and provide a strong motivation for representing this process in ocean general circulation models.

Acknowledgements

KEH was supported by a Ph.D. studentship funded by the Natural Environmental Research Council (NERC Reference NER/S/A/ 2003/11349A). ALMG was supported by the Natural Environment Research Council under NERC Research Grant NE/DO10810/1.

References

Cohen, J. E. and S. E. Belcher (1999). Turbulent shear flow over fast-moving waves. *J. Fluid Mech. 386*, 345–371.

Craik, A. D. D. and S. Leibovich (1976). A rational model for langmuir circulations. *J. Fluid Mech. 73*, 401–426.

D'Asaro, E. A. (2001). Turbulent vertical kinetic energy in the ocean mixed layer. *J. Phys. Oceanogr. 31*, 3530–3537.

Edson, J., T. Crawford, J. Crescenti, T. Farrar, J. Fench, N. Frew, G. Gerbi, C. Helmis, T. Hristov, D. Khelif, A. Jessup, H. Jonsson, M. Li, L. Mahrt, W. McGillis, A. Plueddmann, L. Shen, E. Skyllingstad, T. Stanton, P. Sullivan, J. Sun, J. Trowbridge, D. Vickers, S. Wang, Q. Wang, R. Weller, J. Wilkin, D. Yue, and C. Zappa (2007). The coupled boundary layers and air-sea transfer experiment in low winds. *Bull. Amer. Meteorol. Soc. 88*, 341–356.

Grachev, A. A. and C. W. Fairall (2001). Upward momentum transfer in the marine boundary layer. *J. Phys. Oceanogr. 31*, 1698–1711.

Grant, A. L. and S. E. Belcher (2009). Characteristics of langmuir turbulence in the ocean mixed layer. *J. Phys. Oceanogr.*. submitted.

Hanley, K. E. and S. E. Belcher (2008). Wave-driven wind jets in the marine atmospheric boundary layer. *J. Atmos. Sci. 65*, 2646–2660.

Harris, D. L. (1966). The wave-driven wind. *J. Atmos. Sci. 23*, 688–693.

Kudryavtsev, V. N. and V. K. Makin (2004). Impact of swell on the marine atmospheric boundary layer. *J. Phys. Oceanogr. 34*, 934–948.

Large, W. G., J. C. McWilliams, and S. C. Doney (1994). Oceanic vertical mixing: A review and a model with a nonlocal boundary layer parameterization. *Rev. Geophys.*, 363–403.

Lionello, P., H. Günther, and P. A. E. M. Janssen (1992). Assimilation of altimeter data in a global third-generation wave model. *J. Geophys. Res. 97*, 14,453–14,474.

McWilliams, J. C., P. P. Sullivan, and C. H. Moeng (1997). Langmuir turbulence in the ocean. *J. Fluid Mech. 334*, 1–30.

Polton, J. A. and S. E. Belcher (2007). Langmuir turbulence and deeply penetrating jets in an unstratified mixed layer. *J. Geophys. Res. 112*, doi:10.1029/2007JC004205.

Polton, J. A., D. M. Lewis, and S. E. Belcher (2005). The role of wave-induced Coriolis-Stokes forcing on the wind driven mixed layer. *J. Phys. Oceanogr. 35*, 444–457.

Skyllingstad, E. D. and D. W. Denbo (1995). An ocean large-eddy simulation of langmuir circulations and convection in the surface mixed layer. *J. Geophys. Res. 100*, 8501–8522.

Smedman, A. S., U. Högström, H. Bergstrom, A. Rutgersson, K. K. Kahma, and H. Pettersson (1999). A case study of air-sea interaction during swell conditions. *J. Geophys. Res. 104*, 25,833–25,851.

Sullivan, P. P., J. B. Edson, T. Hristov, and J. C. McWilliams (2008). Large eddy simulations and observations of atmospheric marine boundary layers above non-equilibrium surface waves. *J. Atmos. Sci. 65*, 1225–1245.

Tennekes, H. and J. L. Lumley (1972). *A First Course in Turbulence*. Cambridge University Press.

Tseng, R. S. and E. A. D'Asaro (2004). Measurements of turbulent vertical kinetic energy in the ocean mixed layer from langrangian floats. *J. Phys. Oceanogr. 34*, 1984–1990.

Uppala, S. M., P. W. Kallberg, A. J. Simmons, and Coauthors (2005). The ERA-40 re-analysis. *Q. J. R. Meteorol. Soc. 131*, 2961–3012.